Acta Crystallographica Section F
Structural Biology and Crystallization Communications
ISSN 1744-3091

Crystallization and preliminary X-ray analysis of mycophenolic acid-resistant and mycophenolic acid-sensitive forms of IMP dehydrogenase from the human fungal pathogen *Cryptococcus*

Carl A. Morrow,[a]‡ Anna Stamp,[a]‡ Eugene Valkov,[a,b] Bostjan Kobe[a,b] and James A. Fraser[a]*

[a]Centre for Infectious Disease Research, School of Chemistry and Molecular Biosciences, The University of Queensland, Brisbane, QLD 4072, Australia, and [b]Institute for Molecular Bioscience, The University of Queensland, Brisbane, QLD 4072, Australia

‡ These authors contributed equally to this work.

Correspondence e-mail: jafraser@uq.edu.au

Received 29 June 2010
Accepted 6 August 2010

Fungal human pathogens such as *Cryptococcus neoformans* are becoming an increasingly prevalent cause of human morbidity and mortality owing to the increasing numbers of susceptible individuals. The few antimycotics available to combat these pathogens usually target fungal-specific cell-wall or membrane-related components; however, the number of these targets is limited. In the search for new targets and lead compounds, *C. neoformans* has been found to be susceptible to mycophenolic acid through its target inosine monophosphate dehydrogenase (IMPDH); in contrast, a rare subtype of the related *C. gattii* is naturally resistant. Here, the expression, purification, crystallization and preliminary crystallographic analysis of IMPDH complexed with IMP and NAD^+ is reported for both of these *Cryptococcus* species. The crystals of IMPDH from both sources had the symmetry of the tetragonal space group *I*422 and diffracted to a resolution of 2.5 Å for *C. neoformans* and 2.6 Å for *C. gattii*.

1. Introduction

Fungal infections of humans are highly refractive to pharmacological intervention because of the similarities in our shared eukaryotic physiology. Emerging drug resistance is further exacerbating this problem, as is the growing cohort of immunocompromised individuals susceptible to opportunistic infections. One such opportunist is *Cryptococcus neoformans*, a basidiomycete yeast that predominantly infects immunocompromised patients and causes fungal meningoencephalitis (Casadevall & Perfect, 1998). Recent figures from the US Centers for Disease Control and Prevention estimate an annual global incidence of cryptococcal meningitis of almost 958 000 cases, resulting in more than 624 000 deaths per year. The vast majority of cases involve AIDS patients in sub-Saharan Africa and mirror the prevalence of HIV in the region (Park *et al.*, 2009). The development of more effective, readily available and cheaper antifungals is therefore a matter of urgency.

Rational drug design was pioneered in the purine metabolic pathway, which has continued to serve as a fertile source of drug targets and therapeutic agents for over fifty years (Elion, 1989). One of the key well studied enzymes from this pathway is inosine monophosphate dehydrogenase (IMPDH), which is the rate-limiting enzyme and catalyses the first committed step of *de novo* GTP biosynthesis: the conversion of inosine monophosphate (IMP) to xanthosine monophosphate (XMP). The mechanism involves two reactions: initially, both IMP and the cofactor NAD^+ bind and IMP is oxidized, forming the covalent intermediate E–XMP*, while NAD^+ is reduced to NADH. The E–XMP* complex undergoes a conformational change and is subsequently hydrolysed to form XMP (Jackson *et al.*, 1977; Kohler *et al.*, 2005; Guillen Schlippe & Hedstrom, 2005; Sintchak *et al.*, 1996). XMP is then converted to guanosine monophosphate (GMP) *via* GMP synthase.

As a rate-limiting central metabolic enzyme, IMPDH is highly expressed in proliferating cells and has become a therapeutic target for antimicrobial, antiproliferative and immunosuppressive treatments (Kaur *et al.*, 2005; Allison & Eugui, 2000; Chen & Pankiewicz, 2007). One such therapeutic agent is mycophenolic acid (MPA), an

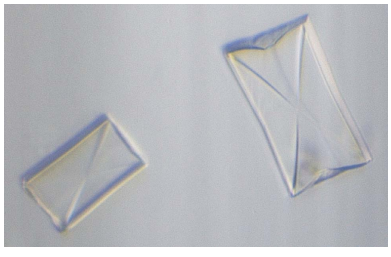

uncompetitive inhibitor of IMPDH that acts as an NAD^+ analogue and traps the covalently bound E–XMP* enzyme intermediate.

IMPDH displays a variability in MPA sensitivity across different species; mammalian enzymes are largely sensitive and in humans MPA acts as a potent immunosuppressant *via* inhibition of B and T lymphocyte proliferation and is commonly prescribed following renal transplantation. Microorganisms, including bacteria, protozoans and fungi, range from extremely sensitive to highly resistant (Hedstrom, 2009; Zhang *et al.*, 1999). Treatment with MPA dramatically reduces the intracellular GTP pool and evokes a range of phenotypes, including abnormal cell morphology, polarity and cell-cycle progression, as well as inhibition of translation and G-protein signalling, in the yeast *Saccharomyces cerevisiae* (Escobar-Henriques *et al.*, 2001; Sagot *et al.*, 2005).

MPA inhibits the growth of *C. neoformans*, yet we have found that a rare subtype of the closely related *C. gattii* is naturally resistant. Kinetic and structural studies have consistently revealed significant differences between microbial IMP dehydrogenases and their human counterparts. Subtle changes in the enzyme conformation, structure of the active site and structure of the cofactor-binding site can lead to substantial changes in IMPDH kinetic parameters and drug resistance, suggesting that highly species-specific inhibitors that do not affect a human host could be developed as novel therapeutics (McMillan *et al.*, 2000; Prosise *et al.*, 2002; Umejiego *et al.*, 2004; Kohler *et al.*, 2005; Riera *et al.*, 2008).

The available structures of eukaryotic IMPDHs include human type I and type II IMPDH and those from *Cricetulus griseus* (Chinese hamster) and a number of protozoan parasites including *Tritrichomonas foetus* and *Cryptosporidium parvum*. The *Cryptococcus* enzymes (both 544 residues) share ∼70% identity with human type I (563 residues) and type II (514 residues) IMPDH, but only ∼44% identity with the well characterized *T. foetus* enzyme (503 residues). *Cryptococcus* IMPDH is slightly longer than most comparable enzymes owing to a unique insertion in part of the active site. No IMPDH structures from the fungal kingdom are available, despite the extensive genetic and biochemical characterization of the enzymes from the model yeast *Saccharomyces cerevisiae* and the human pathogen *Candida albicans* (Shaw *et al.*, 2001; Hyle *et al.*, 2003; Kohler *et al.*, 2005).

To investigate the mechanism of resistance and the potential of *Cryptococcus* IMPDH as an effective therapeutic target, here we describe the crystallization of an MPA-sensitive IMPDH from the clinically prevalent *C. neoformans* and of a rare naturally occurring MPA-resistant IMPDH from *C. gattii*.

2. Materials and methods

2.1. Cloning

Total RNA was isolated from *C. neoformans* var. *grubii* strain H99 and *C. gattii* strain MMRL2651 using TRIzol (Invitrogen, USA). Intron-free cDNA was subsequently synthesized using the Bioline cDNA Synthesis Kit (Bioline, UK) and the IMPDH-encoding *IMD1* gene from both species was PCR-amplified using primers designed to introduce novel restriction sites. The resulting amplicons were digested and cloned in-frame into the pQE-30 expression vector (Qiagen, Netherlands) to introduce an N-terminal 6×His tag (MRGSHHHHHHGS).

The *C. neoformans* strain H99 IMPDH nucleotide sequence (locus designation CNAG_00441) is available from the Broad Institute unpublished genome (http://www.broadinstitute.org/annotation/genome/cryptococcus_neoformans/MultiHome.html), while the *C. gattii* strain MMRL2651 IMPDH sequence is available in GenBank (FJ418781).

2.2. Expression and purification

IMD1 plasmids were cotransformed with the *lac* repressor vector pREP4 into *Escherichia coli* strain BL21 (DE3) pLysS (Novagen, Japan). The transformed cells were grown in LB medium at 310 K with 100 µg ml^{-1} ampicillin and 35 µg ml^{-1} kanamycin to an OD_{600} of ∼1.0 and induced with 1 m*M* IPTG. The cells were subsequently grown for 5 h at 293 K before harvesting. The pellets were resuspended in lysis buffer (50 m*M* HEPES pH 8.0, 1 *M* KCl, 30 m*M* imidazole, 1 m*M* benzamidine–HCl and 1 m*M* PMSF) prior to disruption by sonication. The expressed protein was purified *via* Ni-immobilized metal-affinity chromatography using 5 ml HisTrap columns (GE Healthcare, USA). The supernatant was loaded onto the columns and eluted in a linear gradient of 30–500 m*M* imidazole. Fractions were analysed *via* SDS–PAGE; the peak fractions were concentrated and buffer-exchanged into gel-filtration buffer (50 m*M* Tris–HCl pH 8.0, 150 m*M* KCl, 2 m*M* EDTA, 2 m*M* DTT). Both proteins were loaded onto Superdex 200 size-exclusion columns and eluted at a rate of 2.5 ml min^{-1} using an ÄKTA FPLC system (GE Healthcare). The peak fractions were again identified *via* SDS–PAGE, pooled and concentrated to ∼5 mg ml^{-1} before buffer-exchange into crystallization buffer (50 m*M* Tris–HCl pH 8.0, 50 m*M* KCl, 2 m*M* EDTA, 1 m*M* DTT).

2.3. Crystallization

The optimal protein concentration for crystallization was 5 mg ml^{-1} as determined using the Hampton PCT screen (Hampton Research, USA). For the initial screening, only the IMPDH inhibitor MPA (dissolved in dimethylsulfoxide) was added to a concentration of 100 µ*M* prior to crystallization. Crystallization screening for both proteins was performed using hanging-drop vapour diffusion at 277 K and commercial sparse-matrix screens (Qiagen; Hampton Research; Emerald Biosciences, USA). The plates were set up using a Mosquito Nanodrop crystallization robot (TTP LabTech, UK) by combining 200 nl protein solution and 200 nl reservoir solution and inverting the drops over 100 µl reservoir solution. The drops were monitored and imaged using the Rock Imager system (Formulatrix, USA). An initial crystal cluster was observed for *C. gattii* IMPDH with reservoir solution containing 1.8 *M* lithium sulfate, 6.8%(*v*/*v*) 2-methyl-2,4-pentanediol and 0.09 *M* imidazole–HCl pH 6.5. The crystals were further optimized using factorial grid screening around this condition using sitting-drop vapour diffusion, varying the protein and salt concentration and the pH. In addition, we used an Additive Screen kit (Hampton Research). 1 µl protein solution was mixed with 1 µl reservoir solution and equilibrated against 100 µl reservoir solution. Small crystals obtained in 1.6–1.9 *M* lithium sulfate pH 6.4–6.6 were further optimized by using larger drop sizes and microseeding.

For the final round of crystallization, the IMPDH proteins from *C. neoformans* and *C. gattii* were mixed with a tenfold molar excess of the substrate IMP and the cofactor NAD^+. Large crystals were obtained using wells containing 1.9 *M* lithium sulfate and 0.09 *M* imidazole–HCl pH 6.5 plus either 3.0–12.0%(*v*/*v*) 2-methyl-2,4-pentanediol, 3.0–12.0% pentaerythritol ethoxylate (15/04 EO/OH) or no additive.

2.4. Data collection and processing

Crystals were mounted in nylon loops and immersed in the cryoprotectant Paratone-N (Hampton Research) before flash-cooling in

Table 1
Data-collection and refinement statistics.

Values in parentheses are for the outer shell.

	C. neoformans IMPDH	*C. gattii* IMPDH
No. of crystals	1	1
Beamline	Australian Synchrotron MX2	Australian Synchrotron MX2
X-ray wavelength (Å)	0.95	0.95
Detector	ADSC Quantum 315r	ADSC Quantum 315r
Crystal-to-detector distance (mm)	350	320
Rotation range per image (°)	1	1
Total rotation range (°)	180	180
Exposure time per image (s)	2	2
Data-collection temperature (K)	100	100
Space group	*I*422	*I*422
Unit-cell parameters (Å, °)	$a = b = 148.8$, $c = 106.4$, $\alpha = \beta = \gamma = 90$	$a = b = 148.8$, $c = 106.2$, $\alpha = \beta = \gamma = 90$
Resolution range (Å)	20–2.5 (2.5–2.42)	20–2.6 (2.74–2.6)
Unique reflections	20908	18484
Total observations	305209	491039
$\langle I/\sigma(I)\rangle$	23.6 (4.9)	22.5 (6.1)
$R_{\rm merge}$† (%)	11.7 (78.1)	13.5 (79.6)
$R_{\rm meas} = R_{\rm r.i.m.}$‡ (%)	12.1 (80.9)	13.8 (81.3)
Wilson *B* factor (Å^2)	46.6	52.7
Completeness (%)	99.8 (100)	99.8 (100)
Mosaicity (°)	0.40	0.41
Multiplicity	14.6	26.6
Monomer molecular weight (kDa)	57.9	57.9

† $R_{\rm merge} = \sum_{hkl}\sum_i |I_i(hkl) - \langle I(hkl)\rangle| / \sum_{hkl}\sum_i I_i(hkl)$, where $I_i(hkl)$ is the intensity of an individual measurement of the reflection with Miller indices *hkl* and $\langle I(hkl)\rangle$ is the mean intensity of that reflection. Calculated for $I > -3\sigma(I)$. ‡ $R_{\rm meas} = R_{\rm r.i.m.} = \sum_{hkl}[N/(N-1)]^{1/2}\sum_i |I_i(hkl) - \langle I(hkl)\rangle| / \sum_{hkl}\sum_i I_i(hkl)$, where $I_i(hkl)$ is the intensity of the *i*th individual measurement of reflection *hkl* and $\langle I(hkl)\rangle$ is the weighted average intensity of all measurements *i* of reflection *hkl*. *N* is the multiplicity.

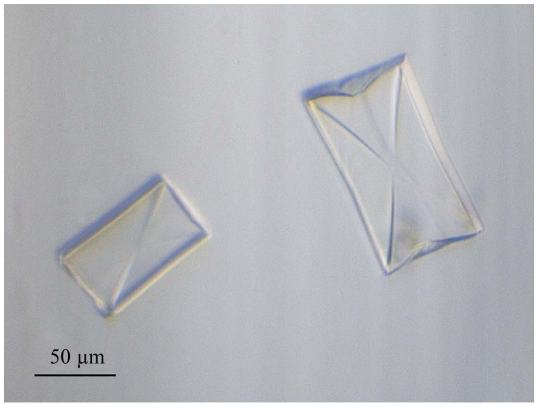

(*a*)

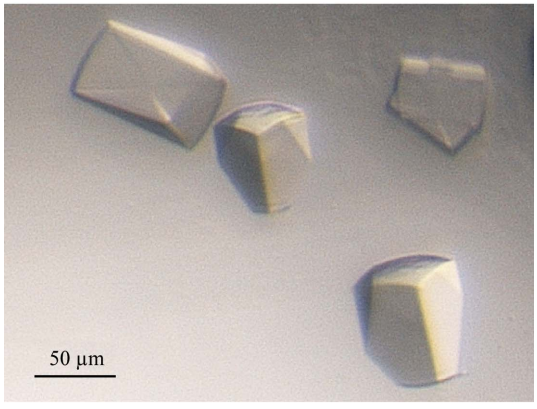

(*b*)

Figure 1
Crystals of cryptococcal IMP dehydrogenases in complex with IMP and NAD$^+$, space group *I*422. (*a*) *C. neoformans* IMP dehydrogenase, (*b*) *C. gattii* IMP dehydrogenase.

liquid nitrogen. Diffraction data were collected from cryocooled single crystals on the MX2 undulator beamline of the Australian Synchrotron (Clayton, Australia). Reflections were indexed and integrated using the program *XDS* (Kabsch, 2010) and then scaled using *SCALA* as implemented within the *CCP*4 suite (Collaborative Computational Project, Number 4, 1994).

3. Results and discussion

Both *C. neoformans* and *C. gattii* IMPDH were expressed heterologously in soluble form in *E. coli* after 5 h induction at 293 K. Both proteins appeared as a single band of approximately 58 kDa on reducing SDS–PAGE gels, matching the estimated size of His-tagged IMPDH monomers, and their purity was estimated to be >99%.

Following initial screening, three further rounds of optimization led to large diffraction-quality crystals in 1.9 *M* lithium sulfate and 0.09 *M* imidazole–HCl pH 6.5 plus either 3–12% 2-methyl-2,4-pentanediol, 3–12% pentaerythritol ethoxylate (15/04 EO/OH) or no further additive. Crystals of both proteins (Fig. 1) appeared after 3 d at 277 K.

The crystals of IMPDH from the two species visually had different morphologies, with the largest IMPDH crystals growing to maximum dimensions of 100 × 150 × 200 µm. However, the crystals of *C. neoformans* and *C. gattii* IMPDH both had the body-centred tetragonal symmetry of space group *I*422. The unit-cell parameters for the *C. neoformans* and *C. gattii* IMPDH crystals were $a = b = 148.8$, $c = 106.4$ Å and $a = b = 148.4$, $c = 106.2$ Å, respectively. The resolution of the best diffracting crystals was 2.5 Å for *C. neoformans* IMPDH and 2.6 Å for *C. gattii* IMPDH. Data-collection and refinement statistics are summarized in Table 1.

Current work is focused on refining the structure of IMPDH for both species and obtaining data sets for alternate ligand-bound forms, including inhibitor-bound MPA-resistant and MPA-sensitive IMPDH.

The authors would like to acknowledge the UQ ROCX facility (The University of Queensland) and the Australian Synchrotron. This work was supported by grants from the National Health and Medical Research Council (NHMRC) and the Australian Research Council (ARC). CAM is supported by an ANZ Trustees PhD Scholarship in Medical Research. JAF is the recipient of an NHMRC Career Development Award. BK is an ARC Federation Fellow and an NHMRC Honorary Research Fellow.

References

Allison, A. C. & Eugui, E. M. (2000). *Immunopharmacology*, **47**, 85–118.
Casadevall, A. & Perfect, J. R. (1998). *Cryptococcus neoformans*. Washington: ASM Press.
Chen, L. & Pankiewicz, K. W. (2007). *Curr. Opin. Drug Discov. Devel.* **10**, 403–412.
Collaborative Computational Project, Number 4 (1994). *Acta Cryst.* D**50**, 760–763.
Elion, G. B. (1989). *Science*, **244**, 41–47.
Escobar-Henriques, M., Balguerie, A., Monribot, C., Boucherie, H. & Daignan-Fornier, B. (2001). *J. Biol. Chem.* **276**, 46237–46242.
Guillen Schlippe, Y. V. & Hedstrom, L. (2005). *Biochemistry*, **44**, 16695–16700.
Hedstrom, L. (2009). *Chem. Rev.* **109**, 2903–2928.
Hyle, J. W., Shaw, R. J. & Reines, D. (2003). *J. Biol. Chem.* **278**, 28470–28478.
Jackson, R. C., Morris, H. P. & Weber, G. (1977). *Biochem. J.* **166**, 1–10.
Kabsch, W. (2010). *Acta Cryst.* D**66**, 125–132.
Kaur, R., Klichko, V. & Margolis, D. (2005). *AIDS Res. Hum. Retroviruses*, **21**, 116–124.
Kohler, G. A., Gong, X., Bentink, S., Theiss, S., Pagani, G. M., Agabian, N. & Hedstrom, L. (2005). *J. Biol. Chem.* **280**, 11295–11302.

McMillan, F. M., Cahoon, M., White, A., Hedstrom, L., Petsko, G. A. & Ringe, D. (2000). *Biochemistry*, **39**, 4533–4542.
Park, B. J., Wannemuehler, K. A., Marston, B. J., Govender, N., Pappas, P. G. & Chiller, T. M. (2009). *AIDS*, **23**, 525–530.
Prosise, G. L., Wu, J. Z. & Luecke, H. (2002). *J. Biol. Chem.* **277**, 50654–50659.
Riera, T. V., Wang, W., Josephine, H. R. & Hedstrom, L. (2008). *Biochemistry*, **47**, 8689–8696.
Sagot, I., Schaeffer, J. & Daignan-Fornier, B. (2005). *BMC Cell Biol.* **6**, 24.
Shaw, R. J., Wilson, J. L., Smith, K. T. & Reines, D. (2001). *J. Biol. Chem.* **276**, 32905–32916.
Sintchak, M. D., Fleming, M. A., Futer, O., Raybuck, S. A., Chambers, S. P., Caron, P. R., Murcko, M. A. & Wilson, K. P. (1996). *Cell*, **85**, 921–930.
Umejiego, N. N., Li, C., Riera, T., Hedstrom, L. & Striepen, B. (2004). *J. Biol. Chem.* **279**, 40320–40327.
Zhang, R., Evans, G., Rotella, F., Westbrook, E., Huberman, E., Joachimiak, A. & Collart, F. R. (1999). *Curr. Med. Chem.* **6**, 537–543.